Available online at www.sciencedirect.com

ScienceDirect

Proceedings of the Combustion Institute 000 (2022) 1–9

Proceedings of the Combustion Institute

www.elsevier.com/locate/proci

Lattice Boltzmann method with nonreflective boundary conditions for low Mach number combustion

Zhen Wang, Timan Lei, Kai Hong Luo*

Department of Mechanical Engineering, University College London, Torrington Place, London WC1E 7JE, United Kingdom

Received 5 January 2022; accepted 6 November 2022
Available online xxx

Abstract

The paper presents a lattice Boltzmann (LB) method for premixed and nonpremixed combustion simulations with nonreflective boundary conditions, in contrast to Navier–Stokes solvers or hybrid schemes. The current approach employs different sets of distribution functions for flow, temperature and species fields, which are fully coupled. The discrete equilibrium density distributions are obtained from the Hermite expansions thus thermal compressibility is included. The coupling among the momentum, energy and species transport enables the model to be applicable for reactive flows with chemical heat release. The characteristic boundary conditions are incorporated into the LB scheme to avoid numerical reflections. The multi-relaxation-time collision schemes are applied to all the LB solution procedures to improve numerical stability. With detailed thermodynamics and chemical mechanisms for hydrogen-air, the LB modelling framework is validated against both premixed flame propagation and nonpremixed counterflow diffusion flame benchmarks. Simulations of circular expanding premixed flames further demonstrate the capability of the new reactive LB method. The developed LB methodology retains the advantages of classic LB methods and extends the LB capability to low Mach number combustion with potential applications in mesoscale and microscale combustors, catalysis, fuel cells, batteries and so on.

Keywords: Lattice Boltzmann method; Reactive flows; Premixed flames; Nonpremixed flames; Numerical simulation

1. Introduction

The lattice Boltzmann (LB) method, which originates from the kinetic theory of gases, has experienced rapid advancement in the past few decades [1,2]. Compared with traditional computational fluid dynamics (CFD) methods, the LB method features several advantages [2]: firstly, it is a more general modelling framework than that based on the Navier–Stokes equations, so that mesoscopic and microscopic features can be easily incorporated; secondly, it has more efficient and easier boundary condition treatments for complex geometries; thirdly, due to its explicit and strictly local formu-

* Corresponding author.
E-mail address: k.luo@ucl.ac.uk (K.H. Luo).

https://doi.org/10.1016/j.proci.2022.11.011

lation, the LB method is extremely efficient for parallel computing [3]. The method therefore has been extensively applied to a variety of complex flow problems, including multiphase flows [2], thermal flows and fluid-structure interactions [4].

LB methods have been less well developed for combustion simulation so far. This is mostly due to the fact the classical iso-thermal LB method is only weakly compressible, and thus the pressure is mainly determined by the local density. Therefore most previous LB-based combustion simulations feature one-way coupling. To correctly account for thermal compressibility in the LB framework, several strategies have been developed in recent years. The first class is the more complex multi-speed LB models [5–8]. The second approach is the "Low Mach Number Approximation model" [9–11]. Alternatively, equilibrium density distribution functions based on thermal Hermite expansion can be used [12–15]. Recent works employing hybrid LB-finite difference models based on the last two approaches have shown promising results [11,16,17]. However, an efficient and robust LB model is still not available for reactive flows with fully coupled flow, temperature/energy and multispecies transport. Furthermore, it has been generally accepted that the multi-relaxation-time (MRT) collision operator can improve the numerical stability of the LB solver compared with the classical single-relaxation-time (SRT) model. Building on the coupled LB models [13,14], the present paper aims to incorporate MRT-LB schemes to solve the flow field, temperature and mass fractions of species in a pure LB formulation, in contrast to the usual LB-finite difference hybrid methods for low Mach number combustion. The details of the model construction are presented in Section 2. The model is validated in Section 3 by considering both premixed and nonpremixed flames. The paper is concluded in Section 4.

2. Numerical method

2.1. MRT-LB model for flow field

The MRT LB model [13] is used to solve the macroscopic Navier–Stokes equations. The model is based on Hermite expansion [13,14]. We apply the method in the standard two-dimensional nine-velocity (D2Q9) LB model. The evolution of the density distribution function is,

$$f_i(\mathbf{x}+\mathbf{e}_i\delta t, t+\delta t) - f_i(\mathbf{x},t) = -\left(\mathbf{M}^{-1}\mathbf{S}\mathbf{M}\right)_{ij}\left[f_j(\mathbf{x},t) - f_j^{eq}(\mathbf{x},t)\right] + \frac{\delta t}{2}\left(C_i(\mathbf{x}+\mathbf{e}_i\delta t, t+\delta t) + C_i(\mathbf{x},t)\right), \quad (1)$$

where $f_i(\mathbf{x},t)$ is the particle distribution function with velocity $\mathbf{e}_i$ at position $\mathbf{x}$ and time t. δt is the lattice time interval. $\mathbf{M}$ represents the orthogonal transformation matrix [13,18] and $\mathbf{S}$ is the diagonal relaxation matrix given by,

$$\mathbf{S} = diag\,(s_0, s_1, s_2, s_3, s_4, s_5, s_6, s_7, s_8). \quad (2)$$

C_i is a correction term to eliminate the deviation from third-order velocity moments [13,14].

Different from the incompressible LB model, the equilibrium density distribution function f_i^{eq} is chosen to be [19,20]:

$$f_i^{eq}(\mathbf{x},t) = w_i\rho\left\{\theta + \frac{\mathbf{e}_i\cdot\mathbf{u}}{c_s^2} + \frac{1}{2c_s^4}\left[(\mathbf{e}_i\cdot\mathbf{u})^2 - c_s^2\mathbf{u}^2\right] + \frac{1}{6c_s^6}\left[(\mathbf{e}_i\cdot\mathbf{u})^3 - 3c_s^2\mathbf{u}^2\right]\right\} \quad (i\neq 0), \quad (3)$$

$$f_i^{eq}(\mathbf{x},t) = w_i\rho\left\{\theta + \frac{1-\theta}{w_i} + \frac{\mathbf{e}_i\cdot\mathbf{u}}{c_s^2} + \frac{1}{2c_s^4}\left[(\mathbf{e}_i\cdot\mathbf{u})^2 - c_s^2\mathbf{u}^2\right] + \frac{1}{6c_s^6}\left[(\mathbf{e}_i\cdot\mathbf{u})^3 - 3c_s^2\mathbf{u}^2\right]\right\} \quad (i=0). \quad (4)$$

For a gas mixture with thermal dilatation effects, θ is the dimensionless temperature defined as $\theta = \bar{r}T/c_s^2$, with $\bar{r} = R\sum_k Y_k/W_k$, and $c_s = \delta x/\delta t/\sqrt{3}$ is the lattice sound speed. R is the gas constant, and Y_k and W_k are the mass fraction and molecular weight of species k, respectively. The improved equilibrium distribution function f_i^{eq} remains positive when θ is small [20], and has shown better numerical stability in simulations of compressible laminar and turbulent flows. Here we apply it to the combustion simulation where large temperature variations exist.

In order to eliminate the implicitness in Eq. (1), $\hat{f}_i = f_i - 0.5\delta t C_i$ is used [13]. The evolution Eq. (1) can be implemented in the moment space as,

$$\mathbf{m}^* = \mathbf{m} - \delta t\mathbf{S}(\mathbf{m}-\mathbf{m}^{eq}) + \delta t\left(\mathbf{I} - \frac{\mathbf{S}}{2}\right)\hat{\mathbf{C}}, \quad (5)$$

where $\mathbf{m} = \mathbf{M}\hat{\mathbf{f}}$, and the equilibrium is,

$$\mathbf{m^{eq}} = \rho\left[1, 2\theta - 4 + 3\mathbf{u}^2, -3\theta + 4 - 3\mathbf{u}^2, u_x, 3u_xu_y^2 - u_x, u_y, 3u_x^2u_y - u_y, u_x^2 - u_y^2, u_xu_y\right]^{\mathrm{T}}. \quad (6)$$

The correction term in moment space is given as,

$$\hat{C} = \Big(0, -3\left(\partial_xQ_x + \partial_yQ_y + \partial_xR_x + \partial_yR_y\right), 3\left(\partial_xQ_x + \partial_yQ_y + \partial_xR_x + \partial_yR_y\right), 0, 0, 0, 0, -\partial_xQ_x + \partial_yQ_y + \partial_xR_x - \partial_yR_y, -\partial_xR_y - \partial_yR_x\Big), \quad (7)$$

with $Q_x = \rho u_x(\theta - 1 + u_x^2)$, $Q_y = \rho u_y(\theta - 1 + u_y^2)$, $R_x = c_s^2\rho u_x(\theta - 1)$, and $R_x = c_s^2\rho u_y(\theta - 1)$.

Please cite this article as: Z. Wang, T. Lei and K.H. Luo, Lattice Boltzmann method with nonreflective boundary conditions for low Mach number combustion, Proceedings of the Combustion Institute, https://doi.org/10.1016/j.proci.2022.11.011

Finally, the macroscopic variables can be calculated as,

$$\rho = \sum_i \hat{f}_i, \quad \mathbf{u} = \frac{\sum_i \mathbf{e}_i \hat{f}_i}{\rho}. \tag{8}$$

Detailed Chapman–Enskog analysis can be found in Li et al. [13]. The shear viscosity in momentum equation is $\mu = (1/s_7 - 0.5)\delta t p$, The ideal gas law $p = \rho \bar{r} T$ then gives,

$$\mu = \left(\frac{1}{s_7} - 0.5\right)\rho \delta t \theta c_s^2. \tag{9}$$

A single relaxation time version of the similar model is used in Feng et al. [16] and Guo et al. [20].

2.2. MRT-LB model for temperature and species fields

The target temperature and mass conservation equations in this study are,

$$\partial_t(\rho c_p T) + \nabla \cdot (\rho c_p T \mathbf{u}) = \nabla \cdot (\lambda \nabla T) + \omega_t, \tag{10}$$

$$\partial_t(\rho Y_k) + \nabla \cdot (\rho Y_k \mathbf{u}) = \nabla \cdot (\rho D_k \nabla Y_k) + \omega_k. \tag{11}$$

Here ω_t and ω_k are the heat release rate and mass production rate due to combustion, respectively. λ is the thermal conductivity of the gas mixture, and D_k is the diffusivity of the species. In line with the recent work on LB-finite difference method [11,16], the current work assumes the diffusion of species obeys the Fick law. For hydrogen-air combustion, the conservation of mass is ensured via a correction to the concentration of nitrogen. Of all 9 species, only 8 species transport equations are solved, and $Y_{N_2} = 1 - \sum_{k=1}^{8} Y_k$.

To solve the above governing equations, MRT LB models are developed with the consideration of the variation of thermophysical properties [21]. The evolution equations are:

$$g_i(\mathbf{x} + \mathbf{e}_i \delta t, t + \delta t) - g_i(\mathbf{x}, t) = -(\mathbf{M}^{-1}\mathbf{S}_t\mathbf{M})_{ij} \left[g_j(\mathbf{x}, t) - g_j^{eq}(\mathbf{x}, t)\right] + \delta t \overline{F}_{t,i} + 0.5\delta t^2 \partial_t \overline{F}_{t,i}, \tag{12}$$

$$h_{k,i}(\mathbf{x} + \mathbf{e}_i \delta t, t + \delta t) - h_{k,i}(\mathbf{x}, t) = -(\mathbf{M}^{-1}\mathbf{S}_k\mathbf{M})_{ij} \left[h_{k,j}(\mathbf{x}, t) - h_{k,j}^{eq}(\mathbf{x}, t)\right] + \delta t \overline{F}_{k,i} + 0.5\delta t^2 \partial_t \overline{F}_{k,i}. \tag{13}$$

$F_{t,i}$ and $F_{k,i}$ are source terms [21]. $g_i(\mathbf{x}, t)$ and $h_{k,i}(\mathbf{x}, t)$ are distribution functions for the temperature and the mass fraction of species k, respectively. The corresponding equilibrium distribution functions g_i^{eq} and $h_{k,i}^{eq}$ are given as,

$$g_i^{eq} = w_i T \left[1 + \frac{\mathbf{e_i} \cdot \mathbf{u}}{c_s^2} + \frac{(\mathbf{e_i} \cdot \mathbf{u})^2}{2c_s^4} - \frac{\mathbf{u^2}}{2c_s^2}\right], \tag{14}$$

$$h_{k,i}^{eq} = w_i Y_k \left[1 + \frac{\mathbf{e_i} \cdot \mathbf{u}}{c_s^2} + \frac{(\mathbf{e_i} \cdot \mathbf{u})^2}{2c_s^4} - \frac{\mathbf{u^2}}{2c_s^2}\right]. \tag{15}$$

To avoid discrete lattice effects, the source terms distribution functions are,

$$\overline{F}_{\zeta,\, i} = w_i F_\zeta \left(1 + \frac{\mathbf{e_i} \cdot \mathbf{u}}{c_s^2} \frac{\tau_\zeta - 0.5}{\tau_\zeta}\right), \tag{16}$$

with $\zeta = t,\ k$, and τ_ζ being the relaxation time. The source terms are:

$$F_t = \frac{D_t}{\rho c_p} \nabla T \cdot \nabla(\rho c_p) + T \nabla \cdot \mathbf{u} + \frac{\omega_t}{\rho c_p}, \tag{17}$$

$$F_k = \frac{D_k}{\rho} \nabla Y_k \cdot \nabla \rho + Y_k \nabla \cdot \mathbf{u} + \frac{\omega_k}{\rho}. \tag{18}$$

More details about the transformation to the moment space can be found in Lei et al. [21]. The gradient of a quantity (e.g., T and Y_k) is evaluated using an LB approach from the distribution functions [22].

Finally, the macroscopic temperature and species concentration can be obtained as

$$T = \sum_i g_i, \quad Y_k = \sum_i h_{k,i} \tag{19}$$

The thermal diffusivity D_t and species diffusivity D_k are related to the relaxation times

$$D_t = \delta t c_s^2(\tau_t - 0.5), \quad D_k = \delta t c_s^2(\tau_k - 0.5) \tag{20}$$

2.3. Nonreflective characteristic boundary conditions for LB method

For simulations of reactive flows, the domain boundaries can result in spurious wave reflections of physical information. Here we incorporate a generalized characteristic boundary conditions (CBCs) to the current LB solver, which can suppress wave reflections at the boundary where the local flow direction is not perpendicular to the boundary. The CBC is applied to momentum, temperature, and species conservation equations. The compressible Navier–Stokes and species transport equations for multi-component reacting flows can be transformed into a characteristic form Poinsot and Lele [23], Sutherland and Kennedy [24], Yoo et al. [25]:

$$\begin{aligned}
&\partial_t u_x + \frac{1}{\rho c}\left(L_4^{(x)} - L_1^{(x)}\right) = \frac{1}{\rho c}\left(\mathrm{T}_4^{(x)} - \mathrm{T}_1^{(x)}\right) + d_{u_x} + s_{u_x} \\
&\partial_t u_y + L_3^{(x)} = \mathrm{T}_3^{(x)} + d_{u_y} + s_{u_y}, \\
&\partial_t \rho + L_2^{(x)} + \frac{1}{c^2}\left(L_4^{(x)} + L_1^{(x)}\right) = \mathrm{T}_2^{(x)} + \frac{1}{c^2}\left(\mathrm{T}_4^{(x)} + \mathrm{T}_1^{(x)}\right) \\
&\partial_t p + L_4^{(x)} + L_1^{(x)} = \mathrm{T}_4^{(x)} + \mathrm{T}_1^{(x)} + d_p + s_p \\
&\partial_t Y_i + L_{5i}^{(x)} = \mathrm{T}_{5i}^{(x)} + d_{Y_i} + s_{Y_i},
\end{aligned} \tag{21}$$

where $c = (rT)^{0.5}$ is the speed of the sound, considering the compression work is neglected in this

Please cite this article as: Z. Wang, T. Lei and K.H. Luo, Lattice Boltzmann method with nonreflective boundary conditions for low Mach number combustion, Proceedings of the Combustion Institute, https://doi.org/10.1016/j.proci.2022.11.011

study. d and s are viscous and source terms, T is the transverse derivative term which can be found in Yoo et al. [25].

The wave amplitudes $L_i^{(x)}$ are defined as,

$$\begin{aligned}
L_1^{(x)} &= \frac{1}{2}(u_x - c)(\partial_x p - \rho c \partial_x u_x),\\
L_2^{(x)} &= u_x\left(\partial_x \rho - \frac{1}{c^2}\partial_x p\right),\\
L_3^{(x)} &= u_x \partial_x u_y,\\
L_4^{(x)} &= \frac{1}{2}(u_x + c)(\partial_x p + \rho c \partial_x u_x),\\
L_{5i}^{(x)} &= u_x \partial_x Y_i.
\end{aligned} \tag{22}$$

For the inflow boundary (take $x = 0$ for example), $L_1^{(x)}$ can be computed using Eq. (22), and the rest are:

$$\begin{aligned}
L_2^{(x)} &= \eta_2 \frac{\rho R}{c l_x}(T - T_0) + \mathrm{T}_2^{(x)},\\
L_3^{(x)} &= \eta_3 \frac{c}{l_x}(u_y - u_{y,0}) + \mathrm{T}_3^{(x)},\\
L_4^{(x)} &= \eta_4 \rho c^2 \frac{1 - M^2}{2 l_x}(u_x - u_{x,0}) + \mathrm{T}_4^{(x)},\\
L_{5i}^{(x)} &= \eta_{5i} \frac{c}{l_x}(Y_i - Y_{i,0}) + \mathrm{T}_{5i}^{(x)},
\end{aligned} \tag{23}$$

where η are the relaxation coefficients and take the value of 0.278 as in previous works [25,26]. The subscript 0 represents the prescribed values of inlet variables. In the present study, it is sufficient to specify $L_{5i}^{(x)} = 0$ for the mass fraction of species [25].

The outflow boundary (take $x = l_x$ for example) is given by,

$$\begin{aligned}
L_1^{(x)} = \sigma_1 c \frac{1 - M^2}{2 l_x}(p - p_\infty) - \beta_1\left(\mathrm{T}_1^{(x)} - \mathrm{T}_{1,exact}^{(x)}\right)\\
+ \mathrm{T}_1^{(x)} + V_1^{(x)} + S_1^{(x)},
\end{aligned} \tag{24}$$

where the relaxation coefficient σ_1 is set to 0.25 [23] and β_1 equals to the local Mach number [26]. p_∞ is the target pressure, and M is the maximum Mach number at the boundary, $\mathrm{T}_{1,exact}^{(x)}$ is the steady value of $\mathrm{T}_1^{(x)}$, and σ_1 and β_1 are the relaxation coefficients for pressure and the transverse term, respectively [25]. The rest wave amplitudes can be directly computed using Eq. (22).

With the wave amplitudes known, the physical values at the boundary can be calculated through Eq. (21). To apply the CBC to the LB solver, the equilibrium part of distribution fictions can be calculated using the physical values obtained. And a second-order extrapolation method is then used to get the nonequilibrium parts, following the idea of the nonequilibrium-extrapolation approach [27].

2.4. Thermodynamic properties and chemistry

Detailed thermodynamic properties and reaction chemistry can be incorporated in the present LB framework. In this study, the hydrogen-air combustion is considered using a 12-step skeletal mechanism [28] involving 9 species, as shown in Table 1.

The thermodynamic properties such as heat capacity are specified using the classical NASA polynomials. The thermal diffusivity of the gas mixture D_t, and the diffusivity of species k, D_k are defined using constant Prandtl and Schmidt numbers:

$$D_t = \frac{\mu}{\rho Pr}, \quad D_k = \frac{\mu}{\rho Sc_k}. \tag{25}$$

The dynamic viscosity can be obtained from a power law [16]:

$$\mu = \mu_0\left(\frac{T}{T_0}\right)^\beta. \tag{26}$$

The heat release rate can be calculated from the species mass production rate and standard enthalpy of formation:

$$\omega_t = \sum_k \omega_k \Delta h_{f,k}^0. \tag{27}$$

Parameters used for Eqs. (25) and (26) are those recommended in Cerfacs database [17] and are listed in Table 2.

Table 1
The 12-step skeletal mechanism of hydrogen-air combustion.

1	$H + O_2 \rightleftharpoons OH + O$
2	$H_2 + O \rightleftharpoons OH + H$
3	$H_2 + OH \rightleftharpoons H_2O + H$
4	$H + O_2 + M \rightarrow HO_2 + M$
5	$HO_2 + H \rightarrow 2OH$
6	$HO_2 + H \rightleftharpoons H_2 + O_2$
7	$HO_2 + OH \rightarrow H_2O + M$
8	$H + OM + M \rightleftharpoons H_2O + M$
9	$2H + M \rightleftharpoons H_2 + M$
10	$2HO_2 \rightarrow H_2O_2 + O_2$
11	$HO_2 + H_2 \rightarrow H_2O_2 + H$
12	$H_2O_2 + M \rightarrow 2OH + M$

Table 2
Thermodynamic parameters.

μ_0	1.8405×10^{-5} Pas
β	0.6759
Pr	0.75
Sc_{H}	0.14
Sc_{OH}	0.53
$Sc_{\mathrm{H_2O}}$	0.6
$Sc_{\mathrm{H_2O_2}}$	0.82
$Sc_{\mathrm{H_2}}$	0.21
$Sc_{\mathrm{O_2}}$	0.8
Sc_{O}	0.53
$Sc_{\mathrm{HO_2}}$	0.8
$Sc_{\mathrm{N_2}}$	1.0

Please cite this article as: Z. Wang, T. Lei and K.H. Luo, Lattice Boltzmann method with nonreflective boundary conditions for low Mach number combustion, Proceedings of the Combustion Institute, https://doi.org/10.1016/j.proci.2022.11.011

2.5. Overall coupling of current model

The present model allows the hydrodynamic and thermodynamic quantities to be fully coupled, unlike most previous LB models for combustion. At the beginning of each time step, based on the local temperature T and mass fraction Y_k, the thermal and chemical parameters (ω_t, ω_k, c_p) are calculated first. Then transport properties including viscosity μ, thermal and mass diffusivities D_t, D_k are also computed. Multiple MRT-LB solvers for flow, temperature and species are run in parallel. T and Y_k are also used to calculate the dimensionless temperature θ, which is required for the discrete equilibrium distribution functions in the flow solver. The density and velocity information (ρ, $\mathbf{u}$) are passed from the flow solver to the temperature and species LB models.

3. Validation of the reactive LB method

To validate the above new LB method for combustion, we first consider the classical one-dimensional (1D) flame propagation, and then the two-dimensional (2D) counterflow diffusion flame. The third validation case is the premixed circular expanding flame.

3.1. 1D flame propagation

For the pseudo-1D flame propagation case, the domain has a left inlet and a right outlet in the x-direction, with periodic boundary conditions in the y-direction. At the left inlet, the fresh gas velocity and mass fractions are fixed, and the temperature is set to 300 K. At the outlet, the CBC described in Section 2.3 is used to set the outlet pressure to atmospheric pressure. The grid size and time step are set to 5×10^{-6} m and 2×10^{-8} s, respectively. At the initialization of the simulation, the left and right half of the domain are filled with fresh and burnt gases at different temperatures. The flame propagation speed can be evaluated using the same method in Feng et al. [16]. Different equivalence ratios ranging from 0.6 to 2 are considered. The flame temperature and speed are shown in Fig. 1, together with those obtained using Cantera (data available from Cerfacs website [29]). For the stoichiometric case, the mass fraction of species and temperature profiles are also compared with Cantera results in Fig. 2. Very good agreement has been achieved.

To demonstrate the effect of different boundary conditions, the evolution of the flame speed is shown in Fig. 3, with the characteristic boundary conditions and Zou-He pressure boundary condition [30] being used at the outlet. In both cases, the characteristic inflow boundary condition is used to specify the velocity at the inlet. It is seen that Zou-He pressure boundary condition leads to significant oscillation of the flame speed and the simulation does not converge.

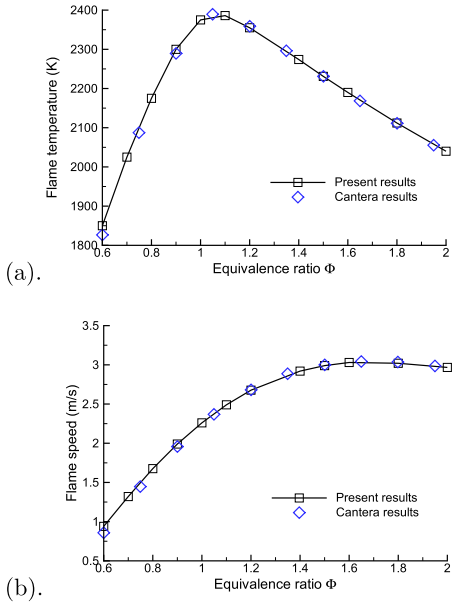

Fig. 1. Flame temperature (a) and speed (b) at different equivalence ratios for hydrogen-air flame propagation. The system pressure is at 1 atm. The results are compared with Cantera results using the same mechanism.

3.2. Nonpremixed counterflow diffusion flame

The 2D nonpremixed counterflow diffusion flame is then simulated. The computational domain is shown in Fig. 4(a) with a dimension of 0.01 m × 0.004 m. The left and right boundaries are fuel and air inlets, respectively. And the top and bottom sides are pressure outlets. The mass fractions of N_2 in the fuel and air are 0.97 and 0.76 respectively. At two inlets, the fuel and air have the same temperature of 300 K and equal mass flow rates. Two strain rates 25 s^{-1} and 50 s^{-1} are considered, which correspond to mass flow rates 0.12 kg m^2 s^{-1} and 0.24 kg m^2 s^{-1}. One example of the temperature and velocity fields are shown in Fig. 4(a). Despite the relatively small domain size compared to the flame thickness, no numerical artefact is visible at any of the boundaries, thanks to the CBC used. The temperature profiles for both strain rates from LB simulations are compared with Cantera calculations in Fig. 4(b), showing good agreement. Note that Cantera uses 'mixture-averaged' transport properties which are different from the constant Prandtl and individual Schmidt numbers (see Section 2.4) in the present study. This may have led to the difference.

Please cite this article as: Z. Wang, T. Lei and K.H. Luo, Lattice Boltzmann method with nonreflective boundary conditions for low Mach number combustion, Proceedings of the Combustion Institute, https://doi.org/10.1016/j.proci.2022.11.011

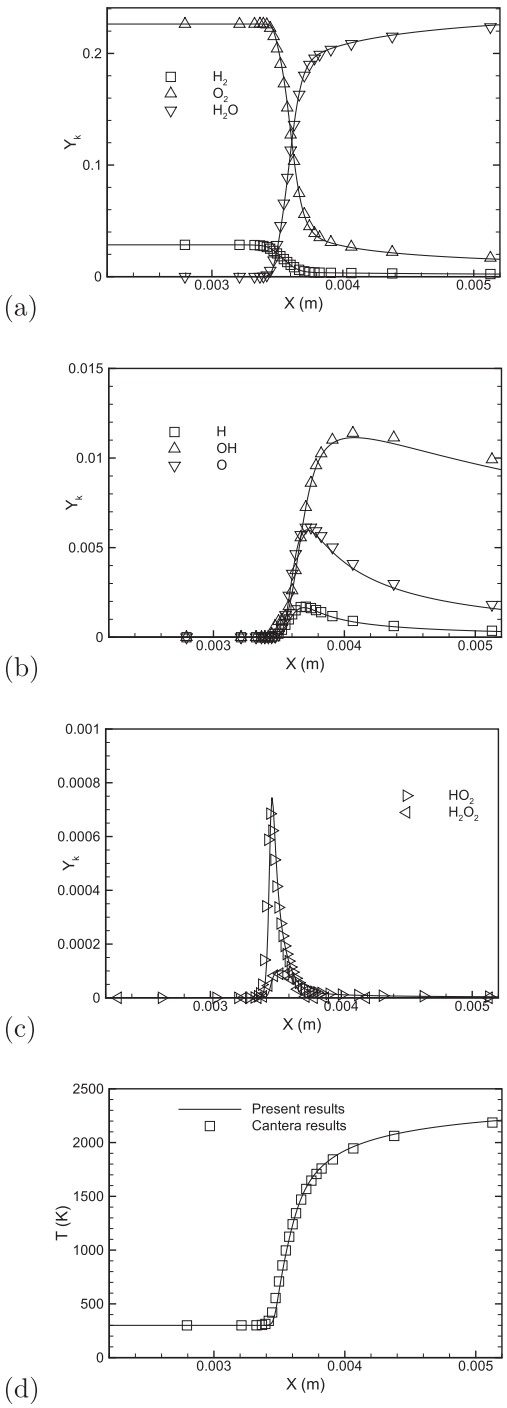

Fig. 2. Mass fraction of species (a) (b) (c) and temperature profile (d) for 1D hydrogen-air flame propagation. The fresh gas is a stoichiometric mixture of hydrogen and air at 1 atm and 300 K. The LB results (lines) are compared with Cantera calculations (symbols).

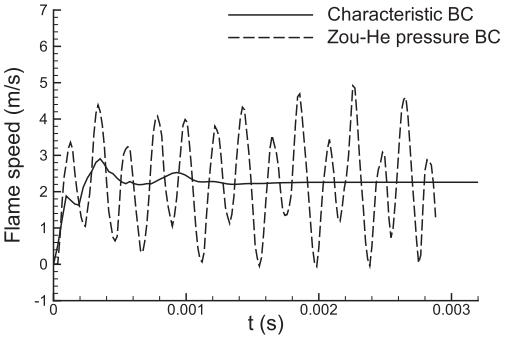

Fig. 3. Comparison of the flame speed when using characteristic boundary conditions and Zou-He pressure boundary condition [30] at the outlet. The fresh gas is a stoichiometric mixture of hydrogen and air at 1 atm and 300 K.

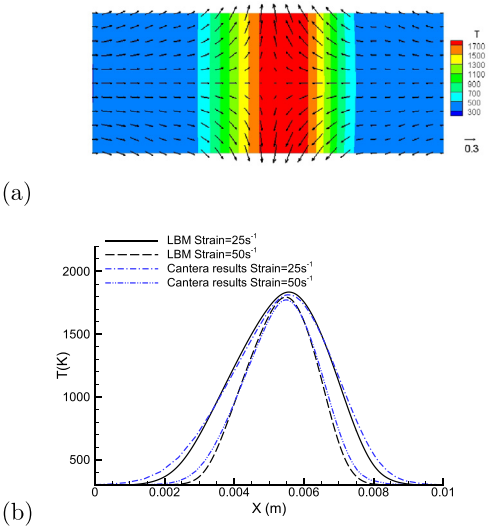

Fig. 4. Hydrogen-air counterflow diffusion flame. The temperature at both inlets are 300 K. Atmospheric pressure. (a) Temperature (K) and velocity fields (m/s), the strain rate is 50 s^{-1}. (b) Temperature along axial direction for two different strain rates, results are compared with Cantera calculations.

3.3. Premixed circular expanding flame

The 2D circular expanding flame is simulated using the present LB model. A lean premixed hydrogen/air mixture with an equivalence ratio of 0.6 is considered at the pressure of 5 atm. The setup is similar to the direct numerical simulation (DNS) work in Altantzis et al. [31] where curved-sided quadrilateral grids were used. A quarter of the flames is simulated as shown in Fig. 5(a). The domain size is 0.01 m × 0.01 m. The CBC is used to apply pressure outflow boundary to the top and

Please cite this article as: Z. Wang, T. Lei and K.H. Luo, Lattice Boltzmann method with nonreflective boundary conditions for low Mach number combustion, Proceedings of the Combustion Institute, https://doi.org/10.1016/j.proci.2022.11.011

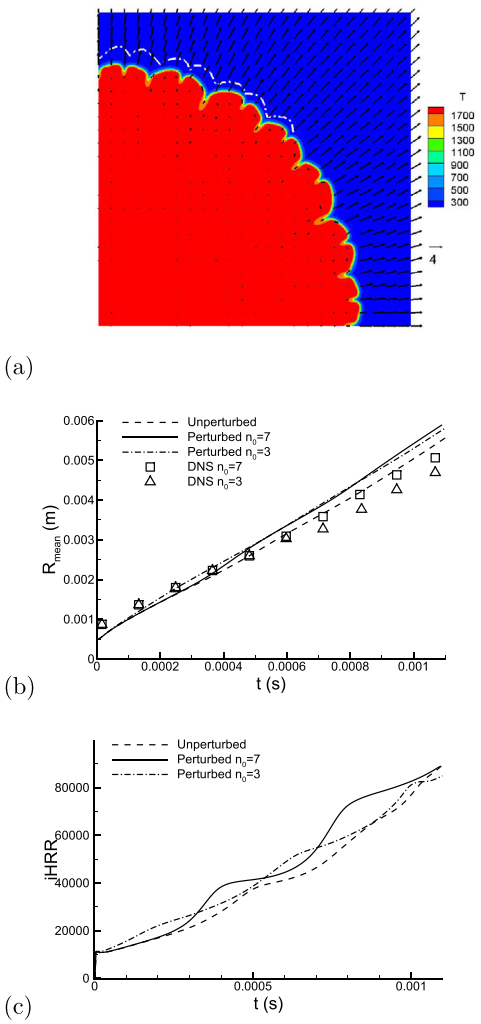

Fig. 5. Premixed circular expanding flame. (a) Temperature and velocity fields at $t = 0.0009$ s for the case with an initialization of 7 cells. The white dash-dot line shows the flame front shape in the DNS simulation when the flame size is similar. Note in Altantzis et al. [31] only the azimuthal direction from $\pi/4$ to $3\pi/4$ is simulated. (b) Comparison of the mean flame radius between the present simulation and the DNS simulation results. (c) Time history of the integral heat release rate.

right sides of the domain, and the left and bottom sides are symmetric boundary conditions. The bottom left corner is initialized with burnt gases at the temperature of 1865 K, and the rest of the domain is initialized with hydrogen/air mixture at the temperature of 298 K. The properties of the burnt gases are obtained from 1D flame simulation.

Three cases are tested. For the first one, the burnt gas is initialized with radius $R_0 = 0.0005$ m. For the other two cases, the flame front is perturbed to $R_0(\theta') = 0.0005(1 + A_0\cos(4n_0\theta'))$, with $A_0 = 0.01$ and $n_0 = 7$ and 3. In the simulation case without perturbation, the flame front remains circular till $t = 0.0003$ s, and then the cells start to form. For the case with an initial perturbation of 7 or 3 cells, flame propagation leads to the splitting of cells into small ones the same as the DNS results in Altantzis et al. [31]. One example can be seen in Fig. 5(a), with the flame shape compared with the DNS simulation.

For all three cases, it can be seen from Fig. 5(b) that the mean flame radius increases linearly, which also agrees with the finding in the DNS. Note that the current configuration is slightly different from the DNS simulation in two main aspects: firstly, a larger value of $A_0 = 0.01$ is used compared to 0.001 in the DNS work, to create effective perturbations, because the present work employs a uniform Cartesian mesh; secondly, the DNS simulation uses a more detailed mechanism. These two aspects may have contributed to the small quantitative difference between LB and DNS simulations in Fig. 5(b).

Finally, Fig. 5(c) shows the integral heat release rate of the expanding flame over the whole domain with $iHRR = \int_A \omega_t$. For the case with no perturbation, $iHRR$ grows linearly with time until later in the simulation. In the perturbed cases, $iHRR$ increases nonmonotonically, which indicates the flame propagation has successive fast and slow periods. These characteristics are similar to the DNS results [31].

4. Discussion and conclusion

We have developed a lattice Boltzmann (LB) model for low Mach number combustion. The validation cases for both premixed flame propagation and nonpremixed counterflow diffusion flame show the accuracy of the present model. Different from recent LB-FD (finite difference) hybrid models [11,16,17], the present modelling framework is purely based on the LB formulations. The thermal compressibility is accounted for, thanks to the Hermite expansion based equilibrium distribution functions. Momentum, temperature and species transport are fully coupled, which makes the current model applicable for more complex reacting flows. The simple structure and explicit nature of the classical LB method are retained in the present method. Although the current model is 2D, the formulations detailed above can be extended to three dimensions straightforwardly.

The MRT schemes are applied to the entire solution process, including separate relaxation times for the hydrodynamic and nonhydrodynamic moments, leading to improved numerical stability compared to SRT schemes. Thus, the present work offers an alternative approach to the recursive regularized collision models [17,20] to apply the Hermite expansion-based equilibrium distribution functions to reactive flow simulations.

Please cite this article as: Z. Wang, T. Lei and K.H. Luo, Lattice Boltzmann method with nonreflective boundary conditions for low Mach number combustion, Proceedings of the Combustion Institute, https://doi.org/10.1016/j.proci.2022.11.011

It is worth noting that treating species and temperature equations using distribution functions requires more computer memory than LB-FD hybrid methods [11,16,17]. On the other hand, a pure LB formulation as developed in this study is computationally efficient on massively parallel computers and can easily treat boundary conditions for complex geometries. Therefore, a unified LB formulation for all equations of combustion simulation, as developed in this study, offers an attractive alternative to traditional combustion simulation methods. The LB-FD formulation [16,17] is another attractive option. In follow-on studies, it would be interesting and important to conduct a rigorous comparison between the pure LB and LB-FD formulations for reactive flow simulations.

The generalized characteristic boundary conditions incorporated into the LB framework have included the transverse derivative terms, and thus can be applied to boundaries where the flow direction is determined by the internal flow field. Wave reflections at the boundary can be eliminated. In all three test cases, the CBC-based outflow boundary can impose accurate pressure and does not affect the flow field inside the computational domain. In our tests, previous LB boundary conditions such as Zou-He [30] and non-equilibrium extrapolation method [27] have failed in these cases, especially for the counterflow flame and circular flame where the local flow direction is not perpendicular to the boundary, as shown in Figs. 4(a) and 5(a).

Finally, the kinetic, mesoscopic nature of the pure LB methodology developed here can easily incorporate mesoscopic and microscopic features that are difficult for conventional Navier–Stokes solvers. This opens up a wide range of application areas such as microscale and mesoscale combustors, catalysis, fuel cells and batteries. Future work will explore these applications, as well as new regimes of combustion.

Declaration of Competing Interest

The authors declare that they have no known competing financial interests or personal relationships that could have appeared to influence the work reported in this paper.

Acknowledgements

Funding from the UK Engineering and Physical Sciences Research Council (EPSRC) under the projects “UK Consortium on Mesoscale Engineering Sciences (UKCOMES)” (Grant no. EP/R029598/1) and “eFlame” (Grant no. EP/S012559/1) is gratefully acknowledged. We thank the referees for their insightful and careful reviews, which have led to improved quality of the paper.

References

[1] S. Chen, G. Doolen, Lattice Boltzmann method for fluid flows, Annu. Rev. Fluid Mech. 30 (1) (1998) 329–364.
[2] Q. Li, K. Luo, Q. Kang, Y. He, Q. Chen, Q. Liu, Lattice Boltzmann methods for multiphase flow and phase-change heat transfer, Prog. Energy Combust. Sci. 52 (2016) 62–105.
[3] D.O. Martinez, W.H. Matthaeus, S. Chen, D. Montgomery, Comparison of spectral method and lattice Boltzmann simulations of two-dimensional hydrodynamics, Phys. Fluids 6 (3) (1994) 1285–1298.
[4] Z.-G. Feng, E. Michaelides, The immersed boundary-lattice Boltzmann method for solving fluid–particles interaction problems, J. Comput. Phys. 195 (2) (2004) 602–628.
[5] C. Lin, K. Luo, L. Fei, S. Succi, A multi-component discrete Boltzmann model for nonequilibrium reactive flows, Sci. Reports 7 (1) (2017) 14580.
[6] C. Lin, K. Luo, Mesoscopic simulation of nonequilibrium detonation with discrete Boltzmann method, Combust. Flame 198 (2018) 356–362.
[7] C. Lin, K. Luo, MRT discrete Boltzmann method for compressible exothermic reactive flows, Comput. Fluids 166 (2018) 176–183.
[8] C. Lin, K. Luo, Discrete Boltzmann modeling of unsteady reactive flows with nonequilibrium effects, Phys. Rev. E 99 (1) (2019) 012142.
[9] S. Chen, Z. Liu, C. Zhang, Z. He, Z. Tian, B. Shi, C. Zheng, A novel coupled lattice Boltzmann model for low Machnumber combustion simulation, Comput. Math. Appl. 193 (1) (2007) 266–284.
[10] O. Filippova, D. Hänel, A novel lattice BGK approach for low Mach number combustion, J. Comput. Phys. 158 (2) (2000) 139–160.
[11] S. Hosseini, H. Safari, N. Darabiha, D. Thévenin, M. Krafczyk, Hybrid lattice Boltzmann-finite difference model for low Mach number combustion simulation, Combust. Flame 209 (2019) 394–404.
[12] N. Prasianakis, I. Karlin, Lattice Boltzmann method for thermal flow simulation on standard lattices, Phys. Rev. E 76 (2007) 016702, doi:10.1103/PhysRevE.76.016702.
[13] Q. Li, K. Luo, Y. He, Y. Gao, W. Tao, Coupling lattice Boltzmann model for simulation of thermal flows on standard lattices, Phys. Rev. E 85 (1) (2012) 016710.
[14] Y. Feng, P. Sagaut, W. Tao, A three dimensional lattice model for thermal compressible flow on standard lattices, J. Comput. Phys. 303 (2015) 514–529.
[15] M. Saadat, F. Bösch, I. Karlin, Lattice Boltzmann model for compressible flows on standard lattices: variable Prandtl number and adiabatic exponent, Phys. Rev. E 99 (1) (2019) 013306.
[16] Y. Feng, M. Tayyab, P. Boivin, A lattice-Boltzmann model for low-Mach reactive flows, Combust. Flame 196 (2018) 249–254.
[17] M. Tayyab, S. Zhao, Y. Feng, P. Boivin, Hybrid regularized lattice-Boltzmann modelling of premixed and non-premixed combustion processes, Combust. Flame 211 (2020) 173–184.
[18] P. Lallemand, L.-S. Luo, Theory of the lattice Boltzmann method: dispersion, dissipation, isotropy, galilean invariance, and stability, Phys. Rev. E 61 (6) (2000) 6546.

Please cite this article as: Z. Wang, T. Lei and K.H. Luo, Lattice Boltzmann method with nonreflective boundary conditions for low Mach number combustion, Proceedings of the Combustion Institute, https://doi.org/10.1016/j.proci.2022.11.011

[19] B.J. Palmer, D.R. Rector, Lattice Boltzmann algorithm for simulating thermal flow in compressible fluids, J. Comput. Phys. 161 (1) (2000) 1–20.
[20] S. Guo, Y. Feng, P. Sagaut, Improved standard thermal lattice Boltzmann model with hybrid recursive regularization for compressible laminar and turbulent flows, Phys. Fluids 32 (12) (2020) 126108.
[21] T. Lei, Z. Wang, K.H. Luo, Study of pore-scale coke combustion in porous media using lattice Boltzmann method, Combust. Flame 225 (2021) 104–119.
[22] T. Lei, X. Meng, Z. Guo, Pore-scale study on reactive mixing of miscible solutions with viscous fingering in porous media, Comput. Fluids 155 (2017) 146–160.
[23] T.J. Poinsot, S. Lele, Boundary conditions for direct simulations of compressible viscous flows, J. Comput. Phys. 101 (1) (1992) 104–129.
[24] J.C. Sutherland, C.A. Kennedy, Improved boundary conditions for viscous, reacting, compressible flows, J. Comput. Phys. 191 (2) (2003) 502–524.
[25] C.S. Yoo, Y. Wang, A. Trouvé, H.G. Im, Characteristic boundary conditions for direct simulations of turbulent counterflow flames, Combust. Theory Model. 9 (4) (2005) 617–646.
[26] C.S. Yoo, H.G. Im, Characteristic boundary conditions for simulations of compressible reacting flows with multi-dimensional, viscous and reaction effects, Combust. Theory Model. 11 (2) (2007) 259–286.
[27] Z.-L. Guo, C.-G. Zheng, B.-C. Shi, Non-equilibrium extrapolation method for velocity and pressure boundary conditions in the lattice Boltzmann method, Chin. Phys. 11 (2002) 366.
[28] P. Boivin, C. Jiménez, A. Sánchez, F. Williams, An explicit reduced mechanism for H_2-air combustion, Proc. Combust. Inst. 33 (1) (2011) 517–523.
[29] Cantera user's guide, 2021. http://www.cerfacs.fr/cantera/mechanisms/hydro.php#boiv.
[30] Q. Zou, X. He, On pressure and velocity boundary conditions for the lattice Boltzmann BGK model, Phys. Fluids 9 (6) (1997) 1591–1598.
[31] C. Altantzis, C.E. Frouzakis, A.G. Tomboulides, K. Boulouchos, Direct numerical simulation of circular expanding premixed flames in a lean quiescent hydrogen-air mixture: phenomenology and detailed flame front analysis, Combust. Flame 162 (2) (2015) 331–344.

Please cite this article as: Z. Wang, T. Lei and K.H. Luo, Lattice Boltzmann method with nonreflective boundary conditions for low Mach number combustion, Proceedings of the Combustion Institute, https://doi.org/10.1016/j.proci.2022.11.011